Hindawi
International Journal of Photoenergy
Volume 2017, Article ID 7153640, 6 pages
https://doi.org/10.1155/2017/7153640

Research Article

Nanostructured Dielectric Layer for Ultrathin Crystalline Silicon Solar Cells

Yusi Chen,[1] Yangsen Kang,[1] Jieyang Jia,[1] Yijie Huo,[1] Muyu Xue,[2] Zheng Lyu,[1] Dong Liang,[3] Li Zhao,[2] and James S. Harris[1,3,4]

[1]*Department of Electrical Engineering, Stanford University, Stanford, CA 94305, USA*
[2]*Department of Material Science and Engineering, Stanford University, Stanford, CA 94305, USA*
[3]*Department of Physics, Stanford University, Stanford, CA 94305, USA*
[4]*Department of Applied Physics, Stanford University, Stanford, CA 94305, USA*

Correspondence should be addressed to James S. Harris; jharris@stanford.edu

Received 18 November 2016; Revised 5 March 2017; Accepted 22 March 2017; Published 16 May 2017

Academic Editor: Sanjay K. Srivastava

Nanostructures have been widely used in solar cells due to their extraordinary photon management properties. However, due to poor pn junction quality and high surface recombination velocity, typical nanostructured solar cells are not efficient compared with the traditional commercial solar cells. Here, we demonstrate a new approach to design, simulate, and fabricate whole-wafer nanostructures on dielectric layer on thin c-Si for solar cell light trapping. The optical simulation results show that the periodic nanostructure arrays on dielectric materials could suppress the reflection loss over a wide spectral range. In addition, by applying the nanostructured dielectric layer on 40 μm thin c-Si, the reflection loss is suppressed to below 5% over a wide spectra and angular range. Moreover, a c-Si solar cell with 2.9 μm ultrathin absorber layer demonstrates 32% improvement in short circuit current and 44% relative improvement in energy conversion efficiency. Our results suggest that nanostructured dielectric layer has the potential to significantly improve solar cell performance and avoid typical problems of defects and surface recombination for nanostructured solar cells, thus providing a new pathway towards realizing high-efficiency and low-cost c-Si solar cells.

1. Introduction

Nanostructures have been widely applied onto solar cells, as they demonstrate promising features for future high-efficiency and low-cost solar cells, such as antireflection and light trapping [1–7]. However, how to effectively realize the potential of nanostructured solar cells still remain a challenge. Compared with traditional commercial counterparts, nanostructured solar cells have lower energy conversion efficiency [8].

On the other hand, ultrathin crystalline silicon (c-Si) solar cells have attracted much interest, as they could potentially achieve high efficiency with low-cost manufacturing [9, 10]. However, due to the intrinsic optical properties of Si as an indirect bandgap material, light trapping using nanostructures is necessary for ultrathin c-Si solar cells to achieve competitive efficiencies [11–14]. In order to get high efficiency, reducing recombination, especially surface recombination, is critical for ultrathin c-Si solar cells [11, 12]. However, typical nanostructured c-Si solar cells suffer from nanostructured pn junction with poor junction quality and high surface damage due the fabrication process, which result in a low V_{oc}, despite a relatively high short circuit current J_{sc} [11–14]. Consequently, the efficiencies of ultrathin c-Si cells are low.

Such problems can be solved in III-V solar cells by nanostructuring the semiconductor window layer with higher energy bandgap instead of nanostructuring the solar cell absorber. The nanostructured window layer could produce antireflection and light-trapping effect, while at the same time maintaining the pn junction quality and blocking the minority carriers from being recombined

at the surface [6]. Similarly, this concept could be applied to c-Si solar cells as well. Particularly, low-cost dielectric materials with large bandgap (above 3 eV) have already been widely used in c-Si solar cells, such as silicon nitride (SiN_x), aluminum oxide (Al_2O_3), and silicon dioxide (SiO_2) [15]. In addition, these dielectric materials have been reported to provide excellent surface passivation for c-Si solar cells [16, 17]. Therefore, by nanostructuring those dielectric materials, antireflection and light trapping could be achieved without sacrificing the junction quality and surface passivation.

In this work, we present the design of nanostructured dielectric layer (NDL) of SiN_x on c-Si thin films for antireflection and light trapping. Simulation and experiment results are also provided and discussed. First, simulation results demonstrate the design robustness and the photon management performance of the NDL over a wide spectra and angular range. Second, NDL is applied onto a 40 μm c-Si thin film, which suppresses the overall reflection to below 5%. In the final part, the NDL is integrated with a c-Si solar cell with 2.9 μm ultrathin absorber layer, demonstrating 32% improvement in J_{sc} and 30 mV enhancement in V_{oc}.

2. Design and Simulation of Nanostructured Dielectric Layer

To study the antireflection effect of nanostructured dielectric layers, optical simulations were performed by finite-difference time-domain (FDTD) method in FDTD Solutions from Lumerical Inc. The simulated nanostructures were an array of nanocones with a 600 nm diameter at the base and 600 nm height, as illustrated in Figure 1. In this simulation, the light source was located above the nanostructures, which is incident normally into the nanostructures. The reflectance of each wavelength was calculated based on the ratio of reflected power and the total incident power. As we are only studying the antireflection effect, the c-Si layer under the NDL is assumed to be infinite. A 10 nm thick SiO_2 (index of 1.6) passivation layer is also included beneath the SiN_x region. When the light comes through the NDL and into the solar cell, reflection occurs at the air/NDL and NDL/c-Si interfaces. The tapper-shaped nanocones provide a gradually changing refractive index and eliminate the reflection at the air/NDL interface. On the other hand, although the index mismatch between dielectric and c-Si exists, SiN_x with refractive index ~ 2 can suppress the reflectance to below 8%.

Figure 2(a) shows the simulated spectral reflectance of SiN_x NDL with refractive index ranging from 1.9 to 2.2. The predicted reflectance is below 10% over a wide portion of the solar spectrum. Another benefit of nanostructures is their wide acceptance angle. Figure 2(b) shows the comparison of simulated spectral averaged reflectance, which is the integrated reflectance weighted by the number of incident photons per wavelength over AM 1.5G, between the SiN_x NDL, single-layer antireflective coating (SLARC, 80 nm thick SiN_x), and double-layer antireflective coating (DLARC). In the simulation, the SLARC was set to be single 80 nm thick

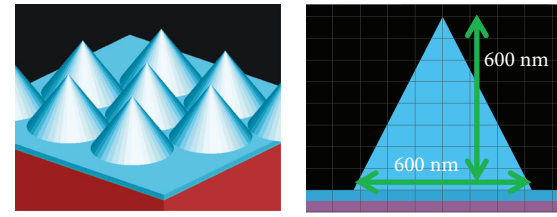

(a) (b)

Figure 1: Schematics of simulated NDL on top of c-Si, including (a) top view and (b) cross section.

SiN_x layer, and the DLARC was 140 nm thick SiO_2 on top of 80 nm thick SiN_x. The SiN_x NDL with refractive index of 2.1 shows below 10% overall reflectance up to 60-degree incidence, which is better than any single-layer antireflective coating (SLARC) at all angles and outperforms double-layer antireflective coating (DLARC) when the incident angle is greater than 20 degrees. On the other hand, the antireflection performance does not change much for NDL with different refractive index from 1.9 to 2.2, which provides a good design robustness as SiN_x might have a variation in refractive index.

3. Fabrication of Nanostructured Dielectric Layer

The SiN_x NDL was fabricated using a nanosphere lithography method [18] as shown in Figure 3. First, 700 nm of SiN_x with 10 nm of SiO_x on top was deposited on the c-Si layer using plasma-enhanced chemical vapor deposition (PECVD) at 350°C. It should be noted that the 10 nm of SiO_x is crucial here for the etching uniformity during the nanosphere lithography process. Next, 600 nm silica nanospheres were assembled into monolayer closed-pack film on top of the SiO_x via Langmuir–Blodgett (LB) coating method [19]. Later, with the silica nanospheres as etch masks, electron cyclotron resonance plasma etching with CF_4 and O_2 gas ($CF_4 : O_2 = 10 : 1$) is used to etch down the SiN_x and produce the nanocone arrays. To achieve isotropic etching for the nanostructures, a high chamber pressure of 40 to 50 mTorr was used [20, 21]. Finally, silica nanosphere residues were removed in 50 : 1 hydrofluoric acid. The shape of nanostructures can be controlled by the ratio between etchant gas and the bias applied during plasma etching. Scanning electron microscope (SEM) images in Figure 4 shows the fabricated nanocone array with different shapes.

4. Nanostructured Dielectric Layer on 40 μm c-Si Layer

To evaluate the antireflection and light-trapping effect, a SiN_x NDL layer was applied onto a 40 μm c-Si thin layer that was prepared using the epi-lift-off (ELO) kerfless Si technique. The NDL layer was fabricated using the method described in Section 3 and has the nanodome shape as in Figure 4(a). The reflectance measurements were performed using a standard integrating sphere system, and the characterization results are shown in Figure 5. Figure 5(a) shows the FDTD

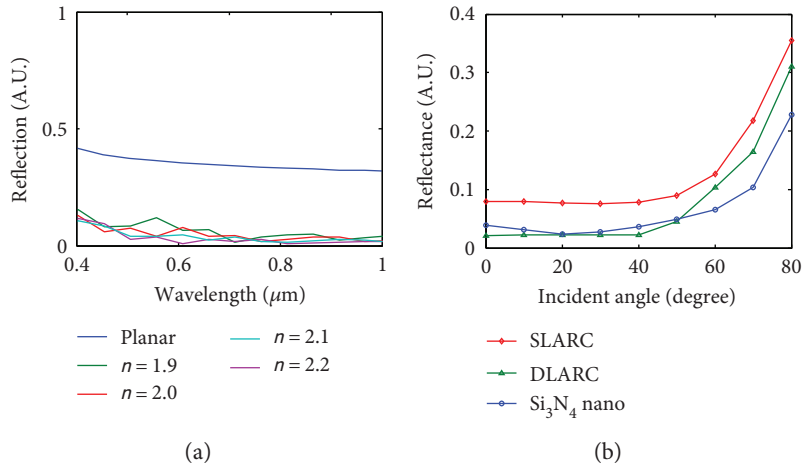

Figure 2: Simulated antireflection properties of SiN_x NDL. (a) Spectral reflectance of SiN_x NDL with refractive index from 1.9 to 2.1 and normal incident light from 300 nm to 900 nm. (b) Simulation result of integrated overall angular reflectance under AM 1.5G of SLARC (red), DLARC (green), and SiN_x NDL with reflective index of 2.1 (blue).

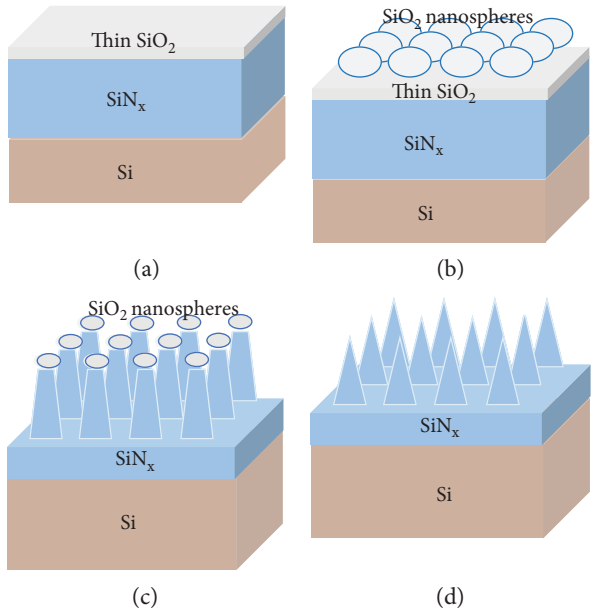

Figure 3: Fabrication process of the SiN_x NDL. (a) Deposit the SiN_x layer on the c-Si, with a thin layer of SiO_x (~10 nm) on top using PECVD; (b) assemble a monolayer of silica nanospheres on top using LB coating method; (c) dry etch the SiN_x with the silica nanospheres as etching masks; and (d) remove the remaining silica nanospheres and SiO_x using wet etch.

simulation and experimental measurement results of reflectance on top of the 40 μm c-Si thin layer with NDL. The incident light is under normal direction with wavelength ranging from 400 nm to 1000 nm. From Figure 5(a), the reflectance loss has been suppressed to below 5% over a wide portion of the solar spectrum, from 400 nm up to 850 nm. Above 850 nm, the reflectance increases for both simulation and measurement results. This is because the optical absorption in c-Si is weak in this wavelength range [22]. The difference between simulation and experiment results at

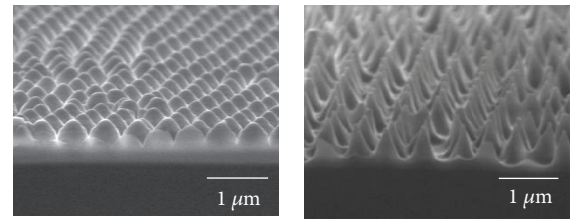

Figure 4: The SEM images of the fabricated NDL with (a) nanodome shape and (b) nanocone shape.

900 nm to 1000 nm mainly comes from the different bottom interface configuration. In simulation, the 40 μm c-Si thin layer is a free-standing thin film and the bottom surface is expose to air with large refractive index mismatch. Therefore, the unabsorbed light gets partially reflected at the bottom surface of c-Si. Such reflected light is reflected again at the front SiN_x/c-Si interface and the SiN_x/air interface. The 40 μm thin Si acts like a resonant cavity in this case, generating the resonant peaks between 900 nm to 1000 nm in Figure 5(a). On the other hand, in experiment, the sample was placed on a thick polymer layer (~1 mm) for handling. Therefore, the reflection from the back surface is not strong enough to generate such resonant peaks as in the simulation results. Figure 5(b) shows the measured integrated reflection at different incident angles. The spectral averaged reflection has been suppressed from ~30% to below 10% up to 60-degree incident angle, demonstrating a wide-angle antireflection effect.

5. Nanostructured Dielectric Layer on Ultrathin c-Si Solar Cells

To better assess the performance of NDL, a c-Si solar cell with 2.9 μm ultrathin absorber was fabricated and integrated with NDL [23]. The fabrication process is shown in Figure 6.

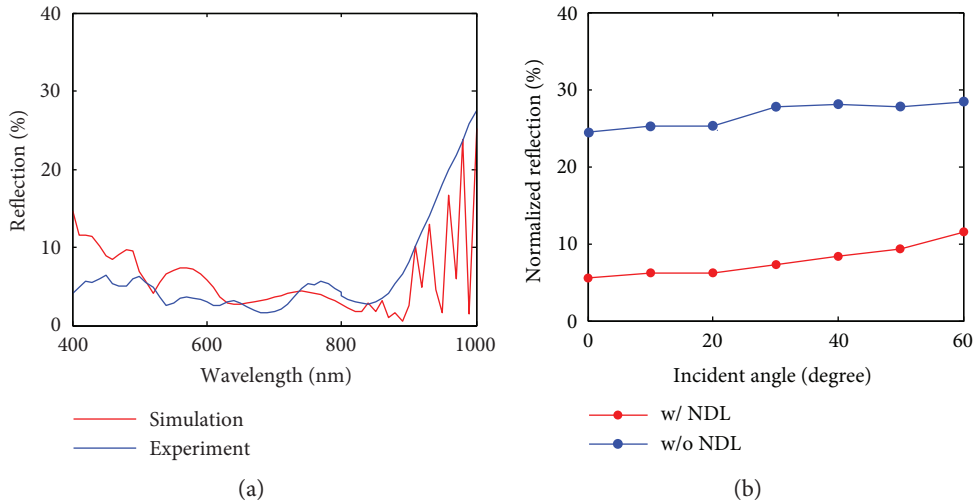

FIGURE 5: (a) The simulation and experiment results of reflection for NDL on 40 μm thick unpolished c-Si. The incident light is at normal direction with wavelength ranging from 400 nm to 1000 nm. (b) The dependence of spectral averaged reflection (400 nm to 1000 nm, AM 1.5G) on incident angle for fabricated NDL on unpolished 40 μm c-Si.

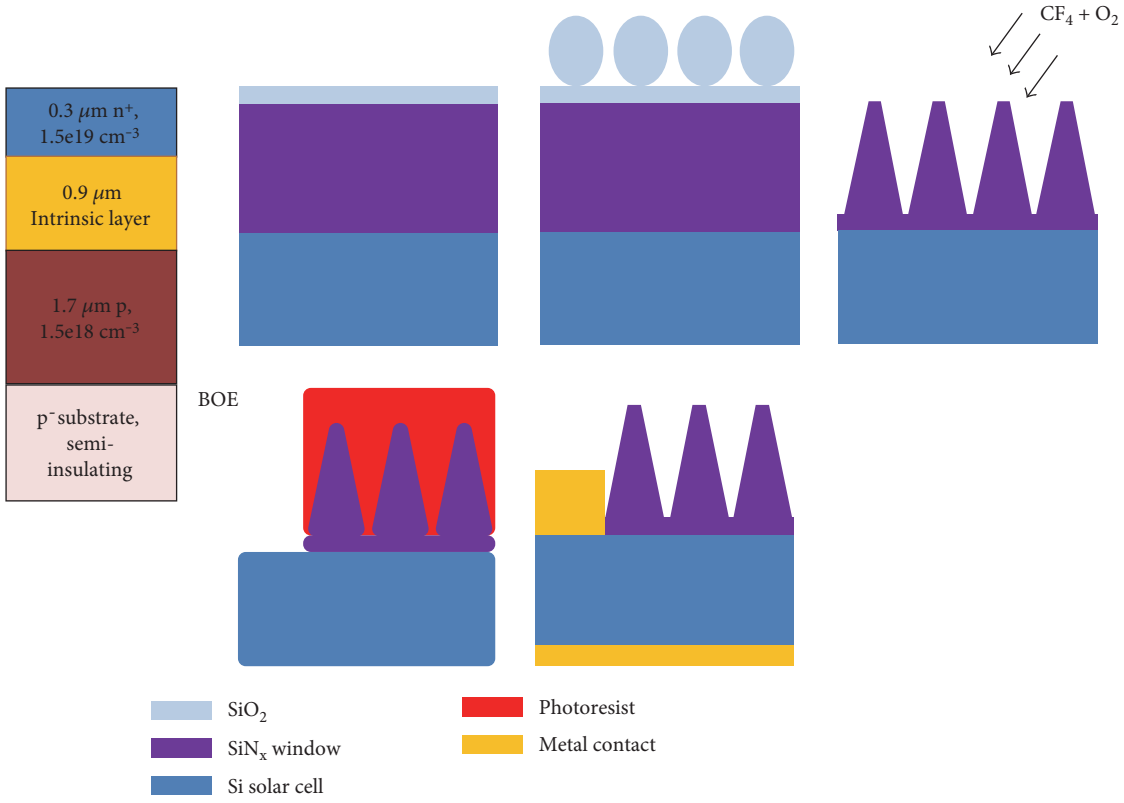

FIGURE 6: Schematics of the fabrication process of ultrathin c-Si solar cells with NDL on top. (a) Deposit a c-Si solar cell with ultrathin absorber on a semi-insulating substrate using RPCVD; (b) deposit the SiN_x layer and thin SiO_x layer on c-Si solar cell; (c) assemble a monolayer of silica nanospheres on top; (d) dry etch the SiN_x layer to form the NDL; (e) use lithography and wet etching of SiN_x in 6 : 1 BOE to define the top contact region; and (f) create front and back metal contacts.

For comparison, a control sample was fabricated using similar process but without the NDL on top.

First, the ultrathin c-Si solar cell was deposited on top of a ~100 Ω·cm semi-insulating p^- CZ substrate using reduced pressure chemical vapor deposition (RPCVD) in an Applied Materials Epi2 system (Figure 6(a)). The deposition was at 1000°C using dichlorosilane (DCS), and phosphine (PH_3) and diborane (B_2H_6) were used as the dopants. The solar cell

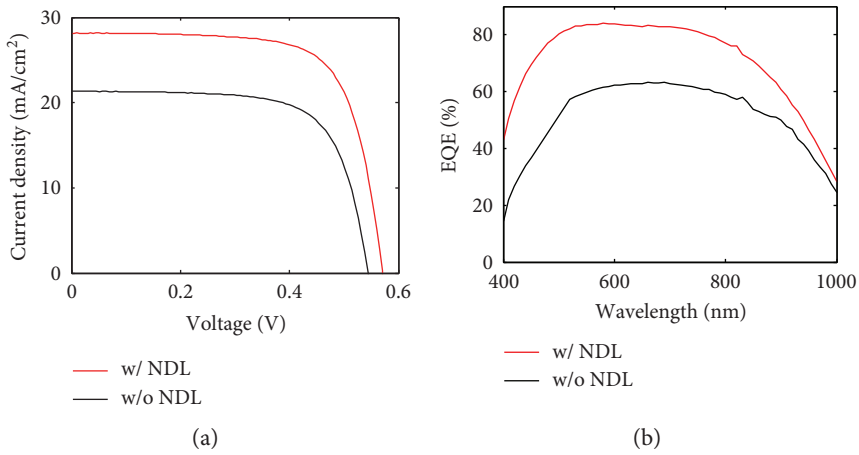

Figure 7: (a) J-V characteristics and (b) EQE characteristics of the solar cells with NDL (red) and without NDL (black).

contains three layers: a 1.7 μm 1.5×10^{18} cm^{-3} boron-doped p-type base layer, a 0.9 μm 10^{16} cm^{-3} p$^-$ intrinsic layer, and a 0.3 μm 1.5×10^{19} cm^{-3} phosphorus-doped n$^+$-type emitter layer.

Second, the NDL was fabricated over the whole sample using the method described in Section 3. 700 nm SiN_x layer was deposited at 350°C using PECVD with 10 nm SiO_x layer on top (Figure 6(b)). Later, a monolayer of compact silica nanospheres was assembled on top of the SiO_x thin film using LB method (Figure 6(c)). Next, a combination of CF_4 and O_2 was used to dry etch the SiN_x with silica nanopheres as etching masks and followed by 50 : 1 HF dip to remove the remaining SiO_x and silica (Figure 6(d)). The fabricated NDL has the nanodome shape as in Figure 4(a).

Standard 5X projection system optical lithography was used to define the contact region. The top contact region is formed by removing the PECVD SiN_x with 6 : 1 buffered oxide etchant (BOE) (Figure 6(e)) and followed by evaporation of 200 nm thick aluminum for the contact. The front contact region is finally formed by lift-off process in acetone. The back contact was formed by directly aluminum evaporation on the back side of the wafer. The schematic of the fabricated solar cell with NDL is shown in Figure 6(f). To evaluate the performance of the NDL, control samples were also fabricated. The control samples have the similar cell structure and fabrication process, but without NDL on top.

The current density-voltage (J-V) characteristics of the fabricated 2.9 μm cells were performed under AM 1.5G 1-sun illumination (1000 W/cm^2) at room temperature. A calibrated solar simulator was used to provide the illumination, and the light intensity was monitored using a NREL certificated solar cell. The J-V measurement results of the cells with and without the SiN_x NDL structures are shown in Figure 7(a), and the key solar cell parameters including short-circuit current density, open-circuit voltage, efficiency, and fill factor are summarized in Table 1.

First of all, the solar cell with NDL achieved a J_{sc} of 28.15 mA/cm^2, which is 32% higher than the J_{sc} of the control cell without NDL. This is due to the antireflection and light-trapping effect of the NDL. Such effect could also be seen from the results of the external quantum efficiency (EQE) measurement in Figure 7(b), which was conducted using mechanically chopped monochromatic light with the photocurrent measured using a lock-in amplifier. With NDL, the EQE is improved from below 60% to ~80% over a wide range of solar spectrum (500 nm to 800 nm). However, EQE decreases at wavelength above 800 nm due to the weak absorption of c-Si at such wavelength range, and the improvement with NDL is also smaller there. The J_{sc} and EQE could be further improved by making a stand-alone ultrathin c-Si solar cell with integrated back reflector [24].

Table 1: Summary of solar cell performance.

	J_{sc} (mA/cm^2)	V_{oc} (mV)	Fill factor (%)	Efficiency (%)
w/ NDL	28.15	570	71.3	11.44
w/o NDL	21.32	540	69.4	8.08
Relative improvement	25%	6.5%	2.7%	44%

Second, the solar cell with NDL also achieved a V_{oc} of 570 mV, which is 30 mV higher than the V_{oc} of the control cell without NDL. As V_{oc} is related to the overall minority carrier recombination inside the solar cells, a higher V_{oc} indicates that the cell with NDL has a better surface passivation effect while still maintaining the same pn junction quality. Such a surface passivation effect could also be seen from the EQE enhancement at short wavelength (400 nm to 500 nm) in Figure 7(b). With NDL, the EQE is improved from below 20% to above 40% at 400 nm, which is more than 100% relative improvement. For photons at 400 nm wavelength, the absorption depth is only 82 nm [22], which means that most of the photons at 400 nm are absorbed near the surface and are highly affected by the surface recombination. Therefore, such a huge improvement at 400 nm EQE not only exhibits the antireflection effect but also demonstrates the surface passivation effect of NDL.

Overall, the solar cell with NDL has an energy conversion efficiency of 11.44%, which is 44% relatively higher than the efficiency of the control cell without NDL.

6. Summary

To summarize, we have demonstrated a systematical analysis of SiN_x NDL for antireflection and light trapping in ultrathin c-Si solar cells. A complete large-area and whole-wafer process to form NDL on thin c-Si is also presented. Also, the NDL has been successfully integrated onto a 40 μm thin c-Si layer and an ultrathin c-Si solar cell with 2.9 μm absorber. From the simulation and experiment results, a wide-spectrum and wide-angle antireflection and light-trapping effect has been achieved using NDL. Together with the good surface passivation effect of SiN_x, NDL exhibits great potential to produce high-efficiency and low-cost ultrathin c-Si solar cells.

Conflicts of Interest

The authors declare that they have no conflicts of interest.

Acknowledgments

This work was supported by the Bay Area Photovoltaic Consortium (BAPVC) and the Global Climate and Energy Project (GCEP) at Stanford University. The authors acknowledge the Stanford Nanofabrication Facility (SNF) for the use of the processing facilities, Center on Nanostructuring for Efficient Energy Conversion (CNEEC) for the use of characterization facilities, and Solexel Inc. for providing the 40 μm c-Si layer. Yusi Chen would like to acknowledge the funding support from Applied Materials Inc. through the SystemX FMA program. Jieyang Jia would like to acknowledge the funding support from the Stanford Graduate Fellowship (SGF).

References

[1] E. Garnett and P. D. Yang, "Light trapping in silicon nanowire solar cells," *Nano Letters*, vol. 10, no. 3, pp. 1082–1087, 2010.

[2] P. J. Poole, D. Dalacu, J. Lefebvre, and R. L. Williams, "Selective epitaxy of semiconductor nanopyramids for nanophotonics," *Nanotechnology*, vol. 21, no. 29, article 295302, 2010.

[3] D. Liang, Y. Huo, Y. Kang et al., "Optical absorption enhancement in freestanding GaAs thin film nanopyramid arrays," *Advanced Energy Materials*, vol. 2, no. 10, pp. 1254–1260, 2012.

[4] J. Zhu, C. M. Hsu, Z. Yu, S. Fan, and Y. Cui, "Nanodome solar cells with efficient light management and self-cleaning," *Nano Letters*, vol. 10, no. 6, pp. 1979–1984, 2010.

[5] J. Zhu, Z. Yu, G. F. Burkhard et al., "Optical absorption enhancement in amorphous silicon nanowire and nanocone arrays," *Nano Letters*, vol. 9, no. 1, pp. 279–282, 2009.

[6] L. Dong, Y. Kang, Y. Huo, Y. Chen, Y. Cui, and J. S. Harris, "High-efficiency nanostructured window GaAs solar cells," *Nano Letters*, vol. 13, no. 10, pp. 4850–4856, 2013.

[7] F. Khan, S. H. Baek, J. Kaur, I. Fareed, A. Mobin, and J. H. Kim, "Paraboloid structured silicon surface for enhanced light absorption: experimental and simulative investigations," *Nanoscale Research Letters*, vol. 10, no. 1, p. 376, 2015.

[8] Y. Kang, D. Liang, Y. Huo et al., "Design and fabrication of nano-pyramid GaAs solar cell," in *Proceedings 39th IEEE Photovoltaic Specialists Conference*, pp. 3321–3323, Tampa, Florida, USA, 2013.

[9] ITRPV Working Group, *International Technology Roadmap for Photovoltaic*, SEMI, 2014, http://www.itrpv.net/.

[10] D. M. Powell, R. Fu, K. Horowitz, P. A. Basore, M. Woodhouse, and T. Buonassisi, "The capital intensity of photovoltaics manufacturing: barrier to scale and opportunity for innovation," *Energy & Environmental Science*, vol. 8, no. 12, pp. 3395–3408, 2015.

[11] M. S. Branham, W. C. Hsu, S. Yerci et al., "15.7% efficient 10-μm-thick crystalline silicon solar cells using periodic nanostructures," *Advanced Materials*, vol. 27, no. 13, pp. 2182–2188, 2015.

[12] S. Jeong, M. D. McGehee, and Y. Cui, "All-back-contact ultra-thin silicon nanocone solar cells with 13.7% power conversion efficiency," *Nature Communications*, vol. 4, no. 4, p. 2950, 2013.

[13] K. J. Yu, J. S. Park, Y. R. Lee et al., "Light trapping in ultrathin monocrystalline silicon solar cells," *Advanced Energy Materials*, vol. 3, no. 11, pp. 1401–1406, 2013.

[14] J. Oh, H.-C. Yuan, and H. M. Branz, "An 18.2%-efficient black-silicon solar cell achieved through control of carrier recombination in nanostructures," *Nature Nanotechnology*, vol. 7, no. 11, pp. 743–748, 2012.

[15] L. M. Fraas and L. D. Partain, *Solar Cells and their Applications*, vol. 236, John Wiley & Sons, New York, USA, 2010.

[16] A. G. Aberle, "Surface passivation of crystalline silicon solar cells: a review," *Progress in Photovoltaics: Research and Applications*, vol. 8, no. 5, pp. 473–487, 2000.

[17] J. Schmidt, M. Kerr, and A. Cuevas, "Surface passivation of silicon solar cells using plasma-enhanced chemical-vapour-deposited SiN films and thin thermal SiO2/plasma SiN stacks," *Semiconductor Science and Technology*, vol. 16, no. 3, p. 164, 2001.

[18] C. M. Hsu, S. T. Connor, M. X. Tang, and Y. Cui, "Wafer-scale silicon nanopillars and nanocones by Langmuir–Blodgett assembly and etching," *Applied Physics Letters*, vol. 93, no. 13, pp. 133109–133109-3, 2008.

[19] B. O. Dabbousi, C. B. Murray, M. F. Rubner, and M. G. Bawendi, "Langmuir-Blodgett manipulation of size-selected Cdse nanocrystallites," *Chemistry of Materials*, vol. 6, no. 2, pp. 216–219, 1994.

[20] B. E. E. Kastenmeier, P. J. Matsuo, J. J. Beulens, and G. S. Oehrlein, "Chemical dry etching of silicon nitride and silicon dioxide using CF4/O2/N2 gas mixtures," *Journal of Vacuum Science & Technology a*, vol. 14, no. 5, pp. 2802–2813, 1996.

[21] C. Reyes-Betanzo, S. A. Moshkalyov, J. W. Swart, and A. C. S. Ramos, "Silicon nitride etching in high- and low-density plasmas using SF6/O2/N2 mixtures," *Journal of Vacuum Science & Technology a: Vacuum, Surfaces, and Films*, vol. 21, no. 2, pp. 461–469, 2003.

[22] M. A. Green and M. J. Keevers, "Optical properties of intrinsic silicon at 300 K," *Progress in Photovoltaics: Research and Applications*, vol. 3, no. 3, pp. 189–192, 1995.

[23] Y. Chen, Y. Kang, Y. Huo et al., "Nanostructured dielectric layer-a new approach to design nanostructured solar cells," in *2014 IEEE 40th Photovoltaic Specialist Conference (PVSC)*, Denver, Colorado, USA, 2014.

[24] K. X. Wang, Z. Yu, V. Liu, Y. Cui, and S. Fan, "Absorption enhancement in ultrathin crystalline silicon solar cells with antireflection and light-trapping nanocone gratings," *Nano Letters*, vol. 12, no. 3, pp. 1616–1619, 2012.